# Ultrafast Photodissociation Dynamics of Acetone at 195 nm: I. Initial-state, Intermediate, and Product Temporal Evolutions by Femtosecond Mass-Selected Multiphoton Ionization Spectroscopy

**Wei-Kan Chen, Jr-Wei Ho, and Po-Yuan Cheng***

*Department of Chemistry, National Tsing Hua University, Hsinchu, Taiwan, R. O. C.*

*Received: February 24, 2005; In Final Form: May 12, 2005*

The photodissociation dynamics of the acetone $S_2$ (n, 3s) Rydberg state excited at 195 nm has been studied by using femtosecond pump−probe mass-selected multiphoton ionization spectroscopy. For the first time, the temporal evolutions of the initial state, intermediates, and methyl products were simultaneously measured and analyzed for this reaction to elucidate the complex dynamics. Two mechanisms were considered: (1) the commonly accepted mechanism in which the primary dissociation occurs on the first triplet-state surface, and (2) the recently proposed mechanism in which the primary dissociation takes place on the first singlet-excited-state surface. Our results and analyses supported the validity of the new mechanism. On the other hand, the conventional mechanism was found to be inadequate to describe the observed dynamics. The temporal evolution of methyl products arising from the secondary dissociation of hot acetyl intermediates exhibited a very complex behavior that can be ascribed to the combination of a nonuniform initial vibrational distribution and the competition between dissociation and slow intramolecular vibrational redistribution.

## 1. Introduction

Photodissociation leading to more than two fragments represents a class of interesting and yet challenging problems in chemical reaction dynamics. One of the main issues is to understand how the multiple bond-breaking steps are temporally correlated and how the available energy is distributed among the fragments. The photodissociation of simple aliphatic ketones at sufficiently high energy is one example in which the two α-CC bonds can break to produce three fragments: two alky radicals and a carbon monoxide molecule.[1,2] This so-called Norrish type I α-cleavage reaction is one of the most important photochemical reactions.[1−3] Being the simplest aliphatic ketone, the photodissociation of acetone in the ultraviolet region has attracted much attention for decades,[3] partly because it is regarded as a prototype for the Norrish type I reaction[6−20] and partly because of its important roles in atmospheric photochemistry.[4,5] At sufficiently high energies, it is energetically possible to break the two equivalent α-CC bonds, and therefore, the "concertedness" of the two-bond breakage had been an issue of concern.[6−12] Through femtosecond (fs) time-resolved experiments, it has been shown unambiguously that the eliminations of the two methyl groups take place via a stepwise mechanism regardless of the excitation energy.[13−20] However, detailed dissociation pathways at such high energies in acetone have not been fully elucidated, and controversies still remained in the literature.[7−20]

The first absorption band of acetone ($S_0 \rightarrow S_1$) occurs in the spectral region from 330 to 220 nm and is due to the dipole-forbidden n $\rightarrow \pi^*$ transition.[21] The band origin has been observed to locate at 328.6 nm.[22] Previous studies have concluded that, upon excitation to the $S_1$ state, the primary α-CC dissociation occurs on the first triplet-state surface following a fast $S_1 \rightarrow T_1$ intersystem crossing (ISC) step.[12,23] Some authors suggested that the $S_1$ and $T_1$ states are strongly mixed, and therefore, a $\{S_1, T_1\}$ mixed state was used to describe the dissociating species in the literature.[10,12,14−16] The α-CC dissociation threshold on the $T_1$ surface has been reported to be at 305.8 nm on the basis of a sudden fluorescence yield decrease at this wavelength,[23,24] and the barrier to dissociation was estimated to be 56 kJ/mol on the $T_1$ surface.[23,24] The resultant hot acetyl radical ($CH_3CO$) may undergo a secondary dissociation to produce $CH_3$ and CO, provided that the internal energy deposited in the acetyl fragment is high enough.

The strong second absorption band ($S_0 \rightarrow S_2$) occurs in the region of 195−180 nm and has been shown to be due to the oxygen $n_0 \rightarrow 3s$ Rydberg excitation.[9,25] Since this is the first strong absorption band in the ultraviolet region, its corresponding photochemistry is expected to play a more important role in the upper atmosphere.[4,5] Excitation of acetone at 193 nm to the $S_2$ state has been reported to produce the three-body products (i.e., $2CH_3 + CO$) with a yield close to unity[11] or greater than 95%.[26] Minor channels, such as $H + CH_2COCH_3$ (∼3%) and $CH_4 + CH_2CO$ (<2%), have also been suggested.[26] A recent study using vacuum UV laser-induced fluorescence detection has reported that the quantum yield for the H-atom elimination channel is about 4%.[27] Gaines et al.[9] have studied the $S_0 \rightarrow S_2$ band with direct absorption spectroscopy under jet-cooled conditions and found the band origin at 195.2 nm. The observations of clear vibronic structures with no underlying continuum had led them to conclude that there exists no direct dissociative states in this spectral region and that the $S_2$ 3s Rydberg state is predissociative.[9]

Many groups[6−10,12,14−16] have studied the photodissociation of the acetone $S_2$ state and provided indirect evidence for a stepwise mechanism.[6−10,12] Baba et al.[6] investigated the photodissociation of actone at 193 nm and suggested the existence of an acetyl intermediate on the basis of the multiphoton ionization power dependence. Woodbridge et al.[7] measured the rotational energy distribution of CO products with time-resolved Fourier transform (FT)-IR emission spectroscopy and concluded that the observed high average rotational energy of CO ($T_{rot}$ = 3360 K) is more consistent with a stepwise mechanism. Trentelman et al.[10] measured the internal and translational energy distributions of $CH_3$ and CO products. The observations of a

* Corresponding author. E-mail: pycheng@mx.nthu.edu.tw.

10.1021/jp050969f CCC: $30.25 
Published on Web 07/14/2005

single component in the $CH_3$ translational energy distribution, a very high rotational energy in CO, and very little vibrational excitation in $CH_3$ led them to conclude that the two bonds cleave in rapid succession on a time scale short enough to allow little redistribution of energy into the methyl degrees of freedom.

North et al.[12] studied the photodissociation of acetone at 193 nm using photofragment translational spectroscopy. Although the observed methyl time-of-flight (TOF) distributions appeared to be a single peak, and no detectable signal was observed in the acetyl mass channel, they have concluded that the reaction proceeds via a stepwise mechanism.[12] Two methyl components were resolved from the overlapped distributions with the assumption that the primary product distribution resembles those measured with 248 and 266 nm photolysis, and the average total translational energies derived from the analyses were 67 and 25 kJ/mol for the primary and secondary dissociations, respectively.[12] The angular distributions of the $CH_3$ and CO fragments were found to be isotropic, suggesting that the overall dissociation is slower than rotation. Because no fragments due to other possible minor channels were observed, they have also concluded that the yield of the three-body dissociation leading to two methyl radicals and a carbon monoxide is near unity.[12]

Kim et al.[13] was the first to carry out fs pump−probe mass-selected multiphoton ionization to study the photodissociation of acetone at a higher Rydberg state, (n, 4s), accessed by two-photon excitation. The observations of the rise and decay of the acetyl intermediate have unequivocally showed that, for the first time, the reactions proceed through a stepwise mechanism. Owrustky and Baronavsky[15,16] performed similar experiments to study $S_2$ 3s Rydberg state dissociation by one-photon excitation at 195 nm. They, too, observed clear acetyl transients and provided the time scales for the reaction.[15,16]

Almost all the above-mentioned studies adopted the commonly accepted notion that the $S_2$ dissociation follows a similar pathway to that in the $S_1$ dissociation,[6−10,12,14−16] that is, fast internal conversion (IC) and ISC processes rapidly bring the molecule to the first triplet state where the dissociation takes place by overcoming a low barrier (see Figure 1).[8−10,12,15,16] Recently, Zewail's group[17−20] reported a series of experimental and theoretical studies for the photodissociation of a variety of linear and cyclic ketones. One of their important findings concerning the acetone photodissociation is that on the acetone $S_1$ surface the barrier to producing a linear acetyl radical in its first electronically excited state, $CH_3CO(\tilde{A})$, is only ∼77 kJ/mol, which is significantly lower than that leading to a bent $CH_3CO(\tilde{A})$.[17−20] This is a direct consequence of the linear equilibrium structure of $CH_3CO(\tilde{A})$.[17] As a result, the adiabatic dissociation on the acetone $S_1$ surface may become more favorable than the slower $S_1 \rightarrow T_1$ ISC at sufficiently high excitation energies. On the basis of these insights, they have proposed a new mechanism for the photodissociation of the acetone $S_2$ state,[19,20] as schematically shown in Figure 1 (solid curved arrows). Briefly, upon excitation to the low-energy region of the $S_2$ state, the molecule first decays to the $S_1$ state via a fast IC step. The primary dissociation of the α-CC bond rapidly occurs on the $S_1$ surface, producing $CH_3CO(\tilde{A})$ and a methyl radical. The electronically excited acetyl radical then relaxes to its ground state and subsequently undergoes a secondary dissociation to produce CO and another $CH_3$. Hereafter, this newly proposed scheme is referred to as the "$S_1$ dissociation ($S_1$D) mechanism", while the commonly adopted one is referred to as the "$T_1$ dissociation ($T_1$D) mechanism". The kinetic expressions of these two mechanisms are shown in Scheme 1.

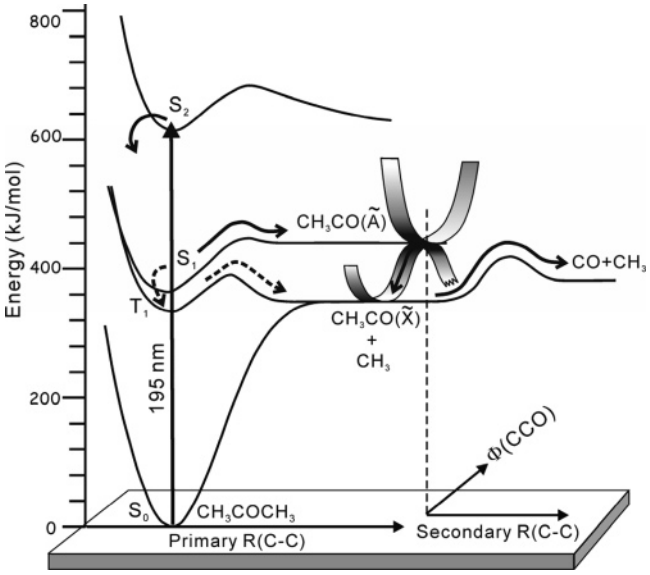


**Figure 1.** Schematic potential energy profiles of relevant states involved in photodissociation of acetone along the primary and secondary α-CC cleavage coordinates. The axis perpendicular to the *R*(C−C) represents the CCO bending coordinate. The energies of stationary points (minima, transition states, and asymptotes) are drawn to scale according to the values reported or adopted in refs 3, 6, 9, 10, and 15−20, but the curves connecting these stationary points are rather arbitrary. The solid curved arrows represent the reaction pathway of the $S_1$D mechanism, whereas the dashed curved arrows illustrate the $T_1$D mechanism, as detailed in the text.

**SCHEME 1: Kinetic Representations of the $T_1$D and $S_1$D Mechanisms**

(A) $T_1$D mechanism

$$AC(S_2) \xrightarrow{k_1} AC(S_1) \xrightarrow{k_2} AC(T_1) \xrightarrow{k_3} CH_3CO(\tilde{X}) + CH_3 \xrightarrow{k_4} CO + CH_3$$

(B) $S_1$D mechanism

$$AC(S_2) \xrightarrow{k_1} AC(S_1) \xrightarrow{k_2} CH_3CO(\tilde{A}) + CH_3 \xrightarrow{k_3} CH_3CO(\tilde{X}) \xrightarrow{k_4} CO + CH_3$$

AC=acetone

It is easy to see that the two mechanisms are simply competing pathways with the branching ratio determined by the rates of $S_1$ adiabatic dissociation and $S_1 \rightarrow T_1$ ISC.

In our previous report,[28] we have provided some preliminary experimental evidence to support the validity of the $S_1$D mechanism. Here, we present a complete account of our studies in elucidating the detailed dynamics of this prototypical photodissociation reaction for alkyl ketones. We excited acetone in a molecular beam with femtosecond (fs) laser pulses at 195 nm to its $S_2$ state near the zero-point level. The temporal evolutions of the initial state, intermediates, and, for the first time, the methyl products were then measured by fs pump−probe mass-selected ionization spectroscopy. The methyl products were probed using 2 + 1 resonance-enhanced multiphoton ionization (REMPI) at 333.5 nm,[29] which provided a definite identification of the products. The result was a complete dynamical picture of the reaction from the initial state to the final products. In the paper that follows,[30] we describe the use of fs time-resolved photofragment translational spectroscopy in studying the methyl-product kinetic energy distributions as a function of reaction time. The combination of these two approaches yielded complementary and consistent results that

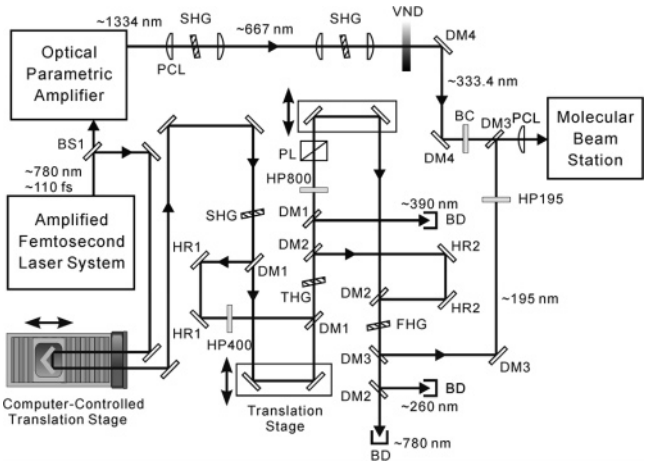


**Figure 2.** Schematic diagram showing the optical setup used in this work. PCL = plano-convex lens; DM = dichroic mirror; HR = high-reflectivity mirror; VND = variable neutral-density filter; SHG/THG/FHG = BBO crystals for harmonic generations; HP = half-wave plate; PL = polarizer; BD = beam dump; BC = Berek compensator.

are crucial in unraveling the complex dynamics in the photodissociation of the acetone $S_2$ state.

## 2. Experimental Section

The fs laser system employed in this work consisted of a self-mode-locked Ti:sapphire laser (Spectra Physics, Tsunami), a 1 kHz chirped-pulse regenerative amplifier (CPA, Spectra Physics, Spitfire) and a five-pass optical parametric generator/amplifier (Light Conversion, TOPAS). A schematic diagram of the optical setup is shown in Figure 2. The oscillator wavelength was tuned to around 780 nm, and the output pulses were selectively amplified in the CPA, producing fs pulses of ~1 mJ/pulse in energy and ~120 fs full width at half-maximum (fwhm) in duration at a repetition rate of 1 kHz. The CPA output was split into two parts by a beam splitter. The major portion (~80%) of the beam was used to pump the optical parametric amplifier, whose signal output at ~1334 nm was subsequently frequency-doubled twice by two thin $\beta$-barium borate (BBO) crystals to produce probe pulses at ~333.5 nm for the 2 + 1 REMPI detection of methyl radicals.[29] With the ~2.5 nm bandwidth, the probe laser covers not only the entire rotational contour of the 3p $^2A_2'' \leftarrow$ 2p $^2A_2'' 0_0^0$ transition of nascent $CH_3$ products but also some nearby hot bands, such as the $1_1^1$ transition.[10] The same 333.5 nm pulses were also used to probe the initial state and acetyl intermediate.

The remaining portion of the CPA output (~20%) was first directed through a retroreflector mounted on a computer-controlled translation stage and was then sent into a harmonic generator to produce the fourth harmonic at ~195 nm, which was used as the pump to excite acetone to the $S_2$ origin region. The optical layout of the harmonic generator is also shown in Figure 2. It produces fs pulses at 195 nm by mixing the CPA output fundamental at 780 nm with the third harmonic at 260 nm in a 0.1-mm-thick BBO crystal. Other probe wavelengths were also used for specific purposes. However, unless otherwise indicated, all transients presented in this work were obtained with a 195 nm pump and a 335.5 nm probe.

The pump and probe beams were collinearly recombined via a dichroic mirror and focused through an $f = 500$ mm lens into the extraction region of a homemade two-stage linear time-of-flight mass spectrometer (TOF-MS) housed in a conventional two-chamber differentially pumped molecular beam apparatus. A 40-mm-diameter microchannel plate (MCP, Burle TOF-4000) assembly located at the end of the 55 cm flight tube was used as the ion detector. An acetone/He gas mixture prepared by flowing pure He gas (~700 Torr) over acetone was expanded through a 75-$\mu$m-diameter pinhole to produce a continuous supersonic jet in the first chamber. The acetone reservoir was immersed in a cold bath kept at ~−40 °C, and the nozzle was heated to ~200 °C to avoid cluster formation. The jet was skimmed before entering the second chamber where it was intersected by the fs laser pulses in the extraction region of the TOF-MS. The molecular beam, laser, and TOF-MS axes are all perpendicular to each other.

A $MgF_2$ half-wave plate and a Berek compensator were used to control the polarization orientations of the pump and probe, respectively, before they entered the molecular beam apparatus. For all transients presented here, the angle between the pump- and probe-laser polarizations was set at the magic angle (54.7°) to minimize any rotational coherence effect. A variable neutral-density filter was placed in the probe beam path to adjust the probe-laser irradiance, while a polarizer−waveplate combination located in the harmonic generator was used to control the pump-laser irradiance. Pulse energies were kept low (~0.1−0.5 $\mu$J/pulse) for the pump laser to ensure one-photon excitation, while slightly higher pulse energies were used for the probe (~0.5−2.0 $\mu$J/pulse) to facilitate multiphoton ionization (MPI). The cross-correlation of the pump and probe pulses was ~270 fs fwhm as determined in situ from the nonresonant pump−probe MPI transient signal near the zero delay time. Femtosecond mass-selected transients were obtained by monitoring the ion intensities of specific mass channels with a boxcar integrator, while the pump versus probe delay time was scanned. Transients were recorded for the parent, acetyl intermediate, and methyl product at masses *m/e* 58 ($CH_3COCH_3^+$), 43 ($CH_3CO^+$), and 15 ($CH_3^+$), respectively.

## 3. Results

**3.1. The Parent Transients.** Figure 3A shows a typical transient obtained by monitoring the parent-ion intensity as a function of pump−probe delay time. The signal rises instantaneously after the pump pulse and then decays slowly in a few picoseconds. The transient can be fit nicely to an exponential decay of 4.2 ± 0.1 ps convoluted with a Gaussian response function of 270 fs fwhm. The pump laser at 195 nm excites acetone to the $S_2$ zero-point energy region. The initially excited state is then ionized by absorbing at least one probe photon at 333.5 nm, reaching a total energy of ~10 eV, which is just above the acetone adiabatic ionization potential (IP) of 9.7 eV (see Figure 5).[31] Owrutsky and Baronavski[15,16] have reported very similar results with a decay of 4.7 ± 0.2 ps for excitation near 194 nm. Because an effusive beam was used in their study, the small discrepancy between the two measurements could be due to the difference in beam temperatures.

Figure 3B shows two normalized parent transients measured with two very different probe-laser pulse energies: 0.2 and 2.0 $\mu$J/pulse. Other experimental conditions were exactly the same. The two transients are nearly identical, and therefore, one of the curves was slightly offset in the figure for the sake of clarity. This observation indicates that within an at least tenfold increase in the probe-laser irradiance, the parent transient does not show any noticeable change in the shape.

**3.2. The Acetyl Transients.** The acetyl transient, shown in Figure 4, also exhibits an instantaneous rise followed by a slow decay. However, close inspections revealed that there is a unique "round-headed" temporal feature in the early-time region (see Figure 4 inset), which should be a manifestation of the

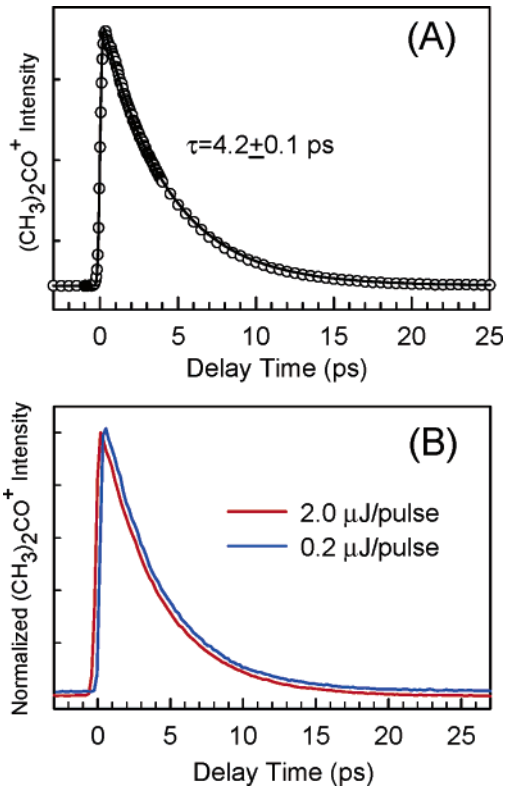


**Figure 3.** (A) Typical transient obtained by monitoring the acetone parent-ion mass (58 amu) signal. The open circles are experimental data, and the solid line is the best fit to an exponential decay convoluted with a Gaussian response function of 270 fs fwhm. (B) Two normalized parent transients measured with probe-laser pulse energies of 0.2 $\mu$J/pulse (blue trace) and 2.0 $\mu$J/pulse (red trace). One of the curves was offset slightly for the sake of clarity, because the two curves are nearly identical.

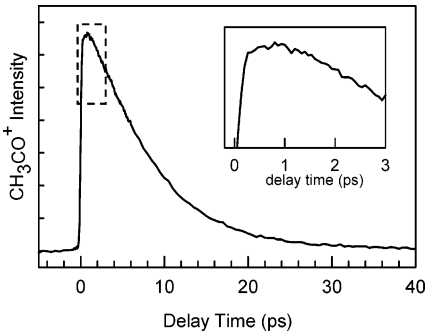


**Figure 4.** Typical transient obtained by monitoring the acetyl ion mass (43 amu) signal. The inset is an enlarged view of the early-time feature highlighted in the dashed box.

underlying complex dissociation pathways. Owrutsky and Baronavski[15,16] have also reported similar acetyl transients for acetone excitation near 194 nm, though their interpretation was different from ours, as discussed below. If the transient shown in Figure 4 arose only from the ionization of neutral $CH_3CO$, then one would expect to observe a rise governed by the 4.2 ps initial-state decay observed in the acetone parent transient (Figure 3). Instead, we observed an instantaneous rise implying that a significant amount of the transient is due to dissociative ionization of the acetone $S_2$ state, as has been proposed previously by others.[14−16] This can occur in the present case, as illustrated in Figure 5, when the initial state absorbs two or more probe photons, producing highly energetic parent ions that decompose into the acetyl ion. Because ionization of the neutral acetyl intermediate requires at least two probe photons at 333

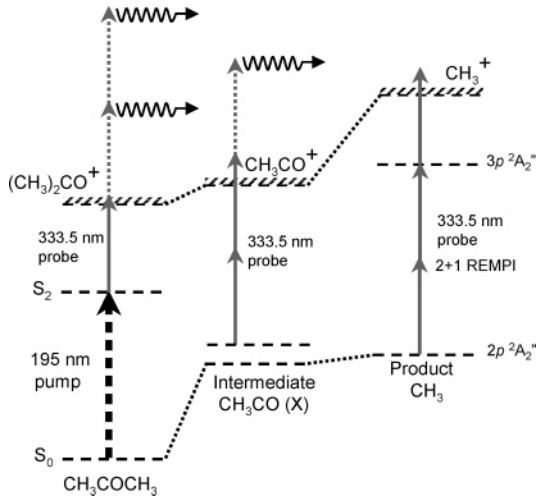


**Figure 5.** Energy level diagram showing photoexcitation of acetone at 195 nm (thick arrow) and ionization of the initial state, intermediate, and products at 333.5 nm (thin arrows). The relative energies of the levels are drawn to scale. The dashed arrows represent absorption of additional probe photon(s) that leads to the dissociative ionization illustrated by the wavy arrows.

nm, two-photon absorption of the evolving acetone $S_2$ state is inevitable under such high probe-laser irradiance. The temporal behavior of this dissociative ionization component should mimic the initial-state decay and must be included in the fits discussed below. We have also measured acetyl transients with a 350 nm probe and found that they are almost identical to those probed at 333.5 nm shown in Figure 4.

**3.3. The Methyl Transients.** Figure 6A shows the methyl transients measured at three probe wavelengths. The 333.5 nm transient (Figure 6A, trace(a)), obtained by using $CH_3$ 2 + 1 REMPI via the 3p $^2A_2'' \leftarrow$ 2p $^2A_2''$ $0_0^0$ transition as the probe, exhibits a nearly instantaneous rise followed by a slow nonexponential rise that reaches a plateau level at ~120 ps. The signal then stays constant up to the longest delay (~1.2 ns) available in this study. The inset in Figure 6A displays a short-time-scale 333.5 nm methyl transient taken with a smaller step size to unfold the early-time behavior. The general rising behavior is consistent with the 2 + 1 REMPI probing scheme employed here for the detection of free $CH_3$ products and is expected to reveal the temporal evolution of the product formation. However, the nearly instantaneous rise in the very-early-time region (<1 ps) is clearly not consistent with the slow decay of a few ps observed for the initial state and the acetyl intermediate. To unravel the complex behaviors of the methyl transients, we also measured a methyl transient with the probe wavelength tuned to 350 nm (Figure 6A, trace (c)), which is completely off any known $CH_3$ REMPI transitions in this spectral region. The 350 nm methyl transient exhibits an instantaneous rise followed by a slow decay that reaches a small but nonzero constant level at ~30 ps. The slow rising behavior observed in the 333 nm transient is now absent in the 350 nm transient. A "round-headed" feature similar to that observed in the acetyl transient is also present in the early-time region of the 350 nm methyl transient, as shown in Figure 6B. Transients taken at other wavelengths off the $CH_3$ REMPI transitions within this general spectral region also gave nearly identical behavior. These observations strongly suggest that the 350 nm (off-resonance) transient is dominated by a nearly wavelength-independent component that should also be present in the 333.5 nm resonance-enhanced transient and is responsible for the instantaneous rise. The small constant signal beyond ~30 ps in the 350 nm transient is probably due to the nonresonant MPI of

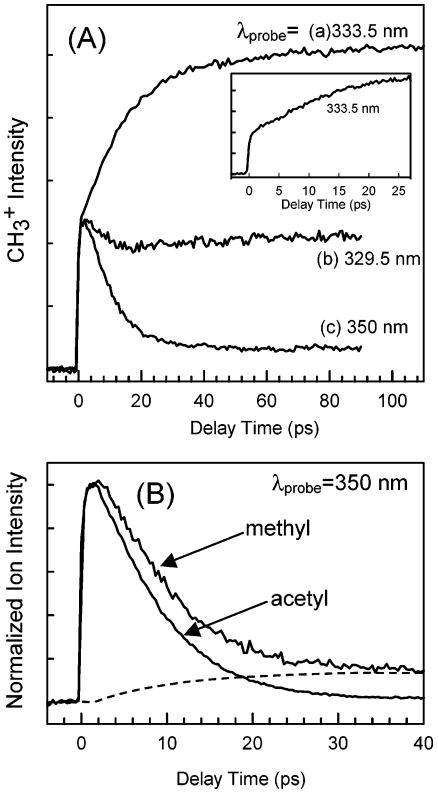


**Figure 6.** (A) Typical transients obtained by monitoring the methyl ion mass (15 amu) signal with $\lambda_{probe}$ = (a) 333.5 nm, (b) 329.5 nm, and (c) 350 nm. Other experimental conditions, including laser irradiances, are similar for all three transients. The independence of the dissociative ionization component on the probe wavelength is evident. The inset shows short-time scale transients taken with $\lambda_{probe}$ = 333.5 nm and a smaller step size to unfold the early-time behavior. (B) Comparisons between a methyl transient taken with $\lambda_{probe}$ = 350 nm and an acetyl transient also taken with $\lambda_{probe}$ = 350 nm. The two transients are normalized to the same maximum intensity. Note the similar "round-headed" features in the early time region of the two transients.

neutral $CH_3$ fragments (dashed trace in Figure 6B), which is greatly enhanced when the probe laser is tuned to 333.5 nm and becomes the much larger slow-rising component. The temporal behavior of this wavelength-independent component in the 350 nm and 333 nm methyl transients is very similar to the acetyl transient, as suggested by the overlaid acetyl transient shown in Figure 6B, and thus can be attributed to the methyl ions arising from the dissociative ionization of initial state and acetyl intermediate. Again, as shown in Figure 5, because ionization of the neutral $CH_3$ radical requires three probe photons at 333.5 nm, two- or three-photon absorption of the evolving acetone $S_2$ state and acetyl intermediate is inevitable under such high probe-laser irradiance used to ionize methyl radicals. This assignment is also supported by the observation of a slightly different probe-laser-irradiance dependence of this wavelength-independent component, which causes the shape of the transient to vary noticeably at much higher probe-laser pulse energies. Further evidence comes from the fs-time-resolved kinetic energy distribution of this temporal component described in the following paper.[30] Thus, even with the REMPI detection, the 333.5 nm methyl transient still contains components arising from dissociative ionization of higher-mass species, and cautions must be taken in analyzing the transients.

We have also measured the growth of the umbrella-mode excited methyl products (Figure 6A, trace(b)) using the $CH_3$ 3p $^2A_2'' \leftarrow$ 2p $^2A_2'' 2_1^1$ hot-band transition at 329.5 nm as the probe.[29] The slow-rising neutral component is still present but is now comparable in size to the dissociative ionization component. Assuming the dissociative ionization component is wavelength-independent within this small spectral range (~333.5−329.5 nm), this observation immediately suggested that the umbrella-mode excited $CH_3$ ($\nu_2 = 1$) is less populated than the vibrationless products. As will be discussed below, the temporal behavior of the umbrella-mode excited $CH_3$ is very similar to that of the cold products and can be described by the same kinetic model with same time constants.

**3.4. Laser-Irradiance and Molecular-Beam Condition Dependencies.** Owing to their high peak powers, fs lasers are tempted to induce multiphoton transitions and other coherent nonlinear processes, which are valuable in many applications, but can become nuisances in fs-laser experiments if they are not well-controlled and understood. We have paid much attention in avoiding such interferences by keeping the laser irradiance at low levels. Careful irradiance dependence studies indicated that all transients presented above are due to one-photon excitation from the pump at 195 nm. The acetyl transients showed a probe-laser irradiance dependence of 1.6 ± 0.3, suggesting that they are due to two-photon ionization by the probe laser. The shapes of the transients do not vary within the range of pulse energies used here: 0.1−0.5 $\mu$J/pulse for the pump and 0.5−2.0 $\mu$J/pulse for the probe. However, at much higher pulse energies, the shapes of transients may vary, and a sharp spike usually appeared at the zero delay time. The former may arise from saturation, multiphoton absorption, and/or strong field effects, while the latter is probably due to enhanced nonresonant MPI when pump and probe pulses overlap in time. All these interferences can be minimized or removed by carefully controlling the laser irradiance in the present case.

The low stagnation pressure (<1 atm He) and small orifice (75 $\mu$m) used in our molecular beam did not encourage the formation of molecular clusters. However, it is well-known that the temporal behaviors of reaction products can be greatly influenced by the caging effect in clusters.[33,34] Accordingly, we have also paid much attention to the molecular beam condition to prevent clustering. In general, no acetone clusters were observed in the TOF-MS spectra with fs MPI under the experimental conditions used to record the transients presented here. Moreover, we have examined the molecular beam condition dependence of the transients and found that their shapes did not change with variation of the nozzle temperatures from 20 to 200 °C and with variation of the acetone reservoir temperatures from +20 to −40 °C. These observations indicate that no acetone clusters were present in the beam, and all transients presented here are due to acetone monomer.

## 4. Analyses and Discussions

The mass-selected fs transients presented above exhibit unique temporal behaviors for the initial-state decay, intermediate evolution, and product formation, which are the manifestation of the underlying complex photodissociation dynamics of the acetone $S_2$ state. A plausible mechanism should be capable of predicting these unique temporal features. In this section, we will discuss the dynamical information elucidated by these mass-selected transients, particularly in relation to the two aforementioned mechanisms.

**4.1. The Parent Transients and the Initial-State Dynamics.** The parent transients shown in Figure 3 exhibit an exponential decay of about 4.2 ps. The initial excitation at 195 nm is to the acetone $S_2$ zero-point region,[9,32] and previous spectroscopic studies have reported vibronically resolved $S_2 \leftarrow S_0$ spectra in

this region with line widths consistent with ps lifetimes.[9,32] Accordingly, we assigned the 4.2 ps decay observed in the parent transient to the lifetime of the acetone $S_2$ state near the zero-point region. As shown in Figure 5, the initially excited $S_2$ state can be ionized by absorbing one probe photon at 333 nm, reaching a total energy of ~10 eV which is just about 0.3 eV above the acetone adiabatic IP.[31] Therefore, the evolution of the parent-ion signal as a function of pump−probe delay time can reflect the $S_2$-state dynamics, consistent with the above assignment. The excitation at 195 nm is much lower than the $S_2$-state dissociation threshold and the predicted $S_2/S_1$ conical intersection.[17−20] High-level ab initio calculations of Diau et al.[17−20] have also suggested that other valence and Rydberg states do not intersect the $S_2$ surface in this region. Therefore, the decay is most likely the result of a Bixon−Jortner type coupling[35] to the lower-lying states. Accordingly, we assigned the 4.2 ps decay to a relatively slow $S_2 \rightarrow S_1$ IC, as has also been proposed by others.[19,20] However, in light of a recent report of ~4% yield for the H-atom elimination arising from $S_0$ dissociation,[27] a small branching from $S_2$ to $S_0$ may also exist. As will be discussed below, the $S_0$ dissociation is expected to be much slower than the time scales observed here; therefore, the following discussion will mainly focus on the subsequent dynamics following the $S_2 \rightarrow S_1$ IC. The rather large energy gap (2.6 eV) between acetone $S_2$ and $S_1$ states is probably responsible for the relatively slow $S_2 \rightarrow S_1$ IC, because the Franck−Condon overlaps between the initially excited $S_2$ levels and the highly vibrationally excited $S_1$ levels are poor. As will be discussed in the following sections, this large energy gap also influences the subsequent dynamics, because the vibrational energy deposited into $S_1$ is enormous.

Because the parent transient is well-described by a single-exponential decay (Figure 3A), the contribution arising from ionization of the vibrationally hot $S_1$ state produced via the $S_2 \rightarrow S_1$ IC must be negligibly small. The hot $S_1$ state component, if present, should exhibit a temporal behavior markedly different from a single-exponential decay and should be resolvable under current time resolution.[36] The negative observation of the hot $S_1$ state is justified, because the energy gap between the acetone $S_2$ and $S_1$ states is extremely large, 2.6 eV (250 kJ/mol), and thus, the internally converted $S_1$ state contains an enormous amount of vibrational energy. Note that this 2.6 eV $S_2-S_1$ energy gap in acetone is much larger than the energy gaps involved in molecular systems where the ionization of hot lower-lying states produced via photophysical steps have been reported.[37−43] On the other hand, it is also larger than the energy gaps in many molecular systems where the ionization of the internally converted lower-lying electronically excited states are not observed.[42,44−47] The 2.6 eV energy gap is comparable to or even greater than the $S_1-S_0$ energy gaps in many large organic molecules, such as azulene,[47] where the ionization of the hot $S_0$ states produced via $S_1 \rightarrow S_0$ IC are not observed.[47−52]

Because the total energy of pump and probe is only 0.3 eV above the acetone adiabatic IP, the very poor Franck−Condon overlaps with the low cationic vibrational levels make one-photon ionization of the highly vibrationally excited $S_1$ levels at 2.6 eV highly unfavorable. The highly vibrationally excited $S_1$ state requires much higher energy to reach the Franck−Condon region in the ion. Such requirements may be met by two-photon absorption of the probe laser. However, as mentioned in section 3.1, we have varied the probe-laser irradiance by at least a factor of 10 (0.2−2.0 $\mu$J/pulse) and found no noticeable changes in the shape of the parent transients (Figure 3B). This indicates that, even under the highest laser irradiance used in this work, multiphoton ionization of the highly vibrationally excited $S_1$ state by the probe laser is unfavorable, or we should have observed some variation in the parent transients shown in Figure 3B. At two-photon ionization level, the total energy is high enough to induce ion fragmentation. However, because the equilibrium structures of the $S_1$ and cationic ground states are quite different,[17−20] ionization of the hot $S_1$ state is expected to produce cations with a broad internal energy distribution. Even if only a small fraction of the parent ions are produced with internal energy below the ion dissociation threshold, their contributions should appear in the parent transient measured at high probe-laser intensities. Furthermore, many previous time-resolved multiphoton ionization studies on $S_2 \rightarrow S_1$ IC dynamics have shown that when hot internally converted $S_1$ states are ionized their contributions appear in the fragment as well as parent-ion mass channels.[38−43] The above observations and arguments suggest that the ionization of the highly vibrationally excited $S_1$ state produced via $S_2 \rightarrow S_1$ IC is unfavorable under current experimental conditions and led us to the assumption applied in the following section that the dissociative ionization of the highly vibrationally excited $S_1$ state can be neglected in the kinetic fittings.

On the other hand, the initially excited $S_2$ levels are those with very low vibrational energies near the zero-point region. Because the $S_2$ state is a Rydberg state, its equilibrium structure is very similar to that of the cationic ground state,[19,20] and thus, the present probing scheme (0.3 eV above adiabatic IP) facilitates a very efficient one-photon ionization for the $S_2$ low vibrational levels. Sequential absorptions via the cold ions may occur and produce highly energetic ions that can dissociate into fragment mass channels and result in the dissociative ionization components observed in the fragment transients.

**4.2. The Acetyl Intermediate: $T_1$D vs $S_1$D Mechanisms.** In this section, we will consider the two aforementioned mechanisms, namely, the $S_1$D and $T_1$D mechanisms, shown in Scheme 1. The kinetics of the two mechanisms can be solved exactly, and the derived temporal functions of each species were then used to fit the experimental transients. Both mechanisms predict an exponential decay for the initially excited $S_2$ state, consistent with the observed parent transient. On the other hand, the two mechanisms predict distinct time dependences for the acetyl intermediate, which can be used to testify to the validity of the dissociation mechanism. Figure 7 shows the comparison between the best fits of the acetyl transient to the two mechanisms. In the fit to the $T_1$D mechanism (Figure 7A), we included an initial-state dissociative ionization component, which is simply an exponential decay of 4.2 ps, and a temporal component for the $CH_3CO(\tilde{X})$ intermediate obtained from solving the kinetics of the $T_1$D mechanism. The reason for including the initial-state dissociative ionization component has been discussed in section 3.2. The dissociative ionization of the vibrationally hot $S_1$ and $T_1$ states is expected to be very inefficient because of very poor Franck−Condon overlaps with the cationic states, a result of the very large $S_2-S_1$ energy gap of 2.6 eV, and was therefore not included in the fits. Experimental supports for this assumption have been discussed in the previous section.

As shown in the Figure 7A inset, it is evident that the $T_1$D mechanism cannot predict the unique "round-headed" temporal feature observed in the acetyl transient. We have also tried other variants of the $T_1$D mechanism, such as treating the $S_1 \rightarrow T_1$ step as a reversible kinetic process or making $S_2$ decay directly to $T_1$ or the mixed $\{S_1T_1\}$ state. However, all attempts based on the $T_1$D mechanism were unsuccessful in fitting the unique "round-headed" temporal feature. These results suggest that the

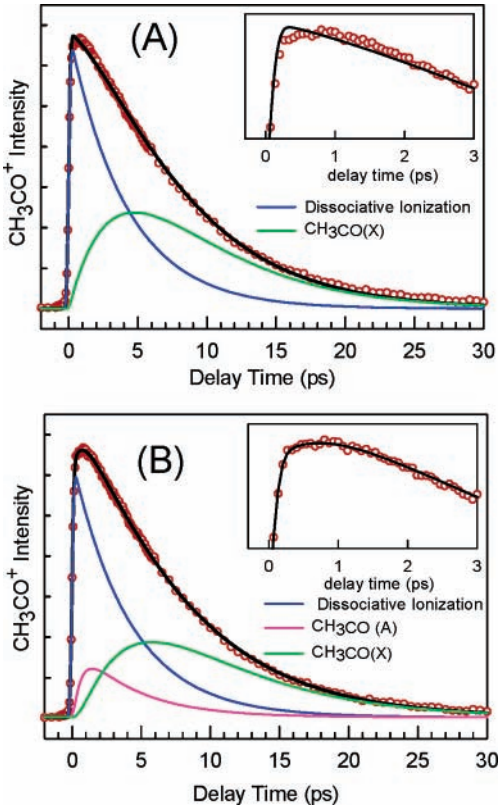


**Figure 7.** Comparisons between the best fits (black lines) of the acetyl transient (red open circles) presented in Figure 3 to (A) the $T_1D$ mechanism and (B) the $S_1D$ mechanism. The insets are enlarged views of the early-time feature highlighted in the dashed box shown in Figure 4. The blue, pink, and green curves represent the decomposed components for the initial-state dissociative ionization, $CH_3CO(\tilde{A})$ and $CH_3CO(\tilde{X})$, respectively.

$T_1D$ mechanism is probably not adequate in describing the photodissociation of the acetone $S_2$ state. On the other hand, the $S_1D$ mechanism produced a nearly perfect fit to the acetyl transient, as shown in Figure 7B. In this case, we included temporal components of the initial-state dissociative ionization and both $CH_3CO(\tilde{A})$ and $CH_3CO(\tilde{X})$ intermediates obtained from solving the kinetics of the $S_1D$ mechanism. The best fits of the parent and acetyl transients to the $S_1D$ mechanism gave the following time constants: $\tau_1 = 4.2 \pm 0.1$ ps, $\tau_2 = 0.6 \pm 0.2$ ps, $\tau_3 = 0.1 \pm 0.05$ ps, and $\tau_4 = 6.2 \pm 0.1$ ps, which are the reciprocals of the corresponding rate constants defined in Scheme 1. The large relative uncertainties for $\tau_2$ and $\tau_3$ arise from the slow initial-state decay and the presence of the dissociative ionization component, which obscure the intermediate ultrafast steps and make more accurate determinations impossible. Moreover, the values of $\tau_2$ and $\tau_3$ can be swapped without affecting the quality of the fits; however, the theoretical considerations described below and the temporal behaviors observed in the time-resolved $CH_3$ kinetic-energy distributions described in the following paper[30] helped to reach the present assignments. These time constants have provided a quantitative picture for the photodissociation dynamics of the acetone $S_2$ state.

In the fits to the $S_1D$ mechanism described above, we have included temporal components for both $CH_3CO(\tilde{A})$ and $CH_3CO(\tilde{X})$ in the model. The acetyl radical $\tilde{X}$ and $\tilde{A}$ states are unique, because they are nearly degenerate at the linear CCO geometry but split along the CCO bending coordinate (see Figures 1 and 8).[19] This is similar to the well-known Renner−Teller effect in the HCO radical, except that the $\tilde{X}$ and $\tilde{A}$ states in HCO are exactly degenerate at linear geometry.[53] This near-

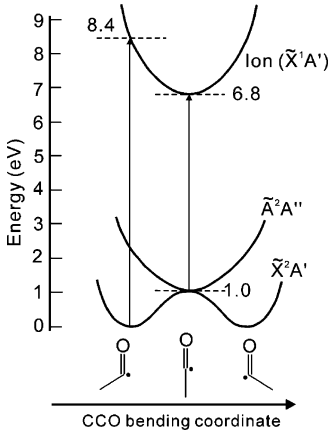


**Figure 8.** Potential energy profiles of the acetyl radical $\tilde{X}$ and $\tilde{A}$ states and acetyl cationic ground state along the CCO bending coordinate (adapted from ref 20).

degeneracy in acetyl radical implies that the vertical IPs of both acetyl $\tilde{X}$ and $\tilde{A}$ states may become very similar near linear geometry and allow $CH_3CO(\tilde{X})$ to be ionized if there is sufficient energy in the CCO bending coordinate. Note that there is no such degeneracy between the acetone $S_1$ and $S_2$ states to bring the vertical IPs of the two states close enough. This effect can be best understood on the basis of the theoretical results reported by Diau et al.[17−20] As shown in Figure 8, $CH_3CO(\tilde{A})$ and the cationic ground state $CH_3CO^+(\tilde{X})$ have nearly parallel potential energy profiles along the CCO bending coordinate, and both assume a linear equilibrium structure. The calculated vertical IP for $CH_3CO(\tilde{A})$ is about 5.8 eV.[19] Consequently, $CH_3CO(\tilde{A})$ can be ionized by absorbing two probe photons at 333.5 nm (3.7 eV). On the other hand, $CH_3CO(\tilde{X})$ has a double-well profile with a bent equilibrium structure. The adiabatic IP of $CH_3CO(\tilde{X})$ was predicted to be 6.8 eV,[19] slightly lower than the experimental value of 7.0 eV.[54] The calculated vertical IP of $CH_3CO(\tilde{X})$, which strongly depends on the CCO bending angle, is 5.8 eV again at 180° but becomes 8.4 eV at the equilibrium angle of 128°.[19,20] If the hot acetyl ground state possesses enough energy in the bending coordinate to get near the linear-geometry region where the vertical IP is lower, then there will be a finite probability that it can be ionized at the two-photon absorption level. This is possible in the present case, because a great portion of the ~1 eV vibrational energy relayed to $CH_3CO(\tilde{X})$ is expected to be initially localized in the bending coordinate because of the large bending angle change upon ultrafast $\tilde{A} \rightarrow \tilde{X}$ IC. However, when the CCO bending energy is dissipated into other modes through intramolecular vibrational energy redistribution (IVR) and the acetyl ground state is trapped in the lower-energy region of the well, the vertical IP of the acetyl ground state may become too high to be reached at the two-photon ionization level (7.45 eV). The above reasoning implies that the decay of the acetyl transient may include contributions from the secondary dissociation and IVR (bending relaxation), which is in line with the complex rising behaviors observed in methyl transients, as discussed below.

The ab inito calculations reported by Diau et al.[19] also predicted that there are three 3p Rydberg states lying in the energy regions accessible by one probe photon (3.7 eV) from the $CH_3CO(\tilde{A})$ and $CH_3CO(\tilde{X})$ states near the linear geometry. It is likely that the ionization of the acetyl radical is resonantly enhanced through these Rydberg states. Because these states are Rydberg in character, their potential energy profiles are very similar to that of the cation along the CCO bending mode, and therefore, resonance occurs only near the linear CCO geometry

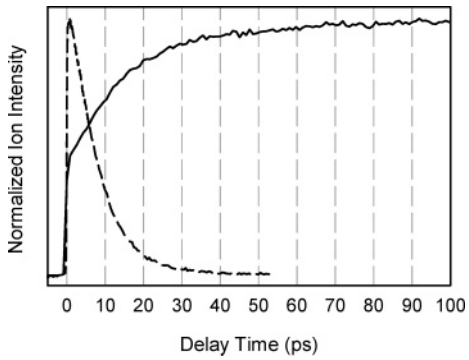


**Figure 9.** Comparisons between a methyl transient and an acetyl transient both taken with $\lambda_{probe} = 333.5$ nm. The two transients are normalized to the same maximum intensity. Note that at ~40 ps the acetyl transient has decayed to the baseline level, while the methyl transient is still rising.

for $CH_3CO(\tilde{X})$. Thus, this probable resonance-enhanced two-photon ionization pathway may enhance the selectivity in ionizing only those $CH_3CO(\tilde{X})$ species with high vibrational energy in the CCO bend.

It is important to emphasize here that the differentiation between the two mechanisms ($T_1D$ vs $S_1D$) described in this section was based on simple kinetic modeling under the assumption that the highly vibrationally excited $S_1$ and $T_1$ levels are not ionized. Thus, although our time-resolved kinetic energy distribution data presented in the following paper[30] also suggest that the $S_1D$ is the dominant dissociation pathway, one should keep in mind that the presence of $T_1D$ branching cannot be ruled out by kinetic modeling.

**4.3. The Methyl Transients: The Comprehensive Fits and an Additional Slow Rise.** We now turn to the methyl transients. In section 3.3, we have shown that, in addition to the neutral $CH_3$ fragment contributions, there is a component arising from dissociative ionization of the initial state and the acetyl intermediate in the methyl transient. The temporal behavior of this component is expected to mimic the acetyl transient, as suggested by the close resemblance between the 350 nm methyl transient and the acetyl transient (see Figure 6). Accordingly, we used an adjustable function simulating the shape of the acetyl transient to describe the dissociative ionization component in the fits. The $S_1D$ mechanism, which has successfully fit the parent and acetyl transients, should be able to describe the temporal behavior of the methyl transient as well. However, fits including the dissociative ionization, primary, and secondary methyl components derived from solving the kinetics of the $S_1D$ mechanism (Scheme 1) with $\tau_1$, $\tau_2$, $\tau_3$, and $\tau_4$ fixed at the values derived from the parent and acetyl transients were found to yield unsatisfactory results. Varying $\tau_4$ while keeping the other three time constants fixed did not satisfactorily improve the fit. Careful comparisons of the methyl and acetyl transients revealed that the methyl product rise is indeed slower than the decay of the acetyl intermediate, as shown in Figure 9, and there seems to exist an additional slower-rise component beyond ~30 ps, that is, the overall rise is approximately biexponential. As mentioned earlier, we have carefully avoided cluster formation in the beam, and therefore, this behavior is not due to the caging effects generally found in molecular clusters.[33,34] This unexpected observation suggests that the observed intermediate decay does not necessarily correlate directly to the product formation! The observed intermediate decay could be simply due to the decrease in the probing efficiency during the dynamical evolution and may not faithfully reflect the population changes of intermediates and products.

This additional slow rise could be due to the existence of some small branching pathways. One possibility is the primary dissociation of the hot $S_0$ state produced by $S_2 \rightarrow S_0$ IC mentioned earlier. This channel might exist, because a recent experiment has shown that there is an ~4% yield of H-atom elimination via acetone $S_0$ dissociation.[27] The H-atom elimination threshold (~400 kJ/mol)[27] is higher than that of the α-CC bond (~350 kJ/mol); therefore, one would expect the primary $S_0$ C−C dissociation to account for at least 4% yield. However, with the total internal energy of 614 kJ/mol and C−C bond energy of 350 kJ/mol in the $S_0$ state, we expect this channel to take place in a much longer time scale than those observed here. A good example is the phototdissociation of dimethyl sulfoxide (DMSO) at 195 nm recently studied in our laboratory.[55] In this case, an $S_0$-dissociation channel has been identified, which exhibits a methyl product rise of ~80 ps. DMSO is of the same size as acetone, but has a much weaker S−C bond energy of 218 kJ/mol. Therefore, the acetone $S_0$ C−C dissociation should take a much longer time than 80 ps at the same energy and is probably not observed here.

Another possible source of this additional long rise is a small branching of the $T_1D$ mechanism. This could occur if the $S_1 \rightarrow T_1$ ISC rate were comparable to the primary dissociation rate on the $S_1$ surface. A discussion concerning the $S_1-T_1$ ISC rate in this energy region will be given in section 4.6, which suggests this pathway to be unlikely. Nevertheless, if it does occur, $T_1$ would possess a higher internal energy and dissociate over a lower barrier (see Figure 1) of ~56 kJ/mol;[23,24] therefore, the dissociation on the $T_1$ surface is expected to be much faster than that in $S_1$. Accordingly, the methyl radicals resulting from the $T_1$ surface, if there were any, would probably exhibit an almost identical temporal behavior to those coming from $S_1$, not slower in time. Further evidence also comes from the fs time-resolved kinetic energy distributions that will be presented in the following paper.[30] Although a very small branching of the $T_1D$ channel cannot be completely ruled out due to the limited *S*/*N* ratio and the complexity of the fits, it certainly cannot account for the additional slow rise.

Another logical modification to the $S_1D$ mechanism in order to account for the additional slow rise is to assume that the hot $CH_3CO(\tilde{X})$ decays to a dark species which then dissociates to form $CH_3$ and CO with a slower rate. One possibility is that a fraction of highly excited intermediates is transformed into the vinoxy radical,[56,57] which then slowly isomerizes back to the acetyl radical and rapidly dissociates into $CH_3$ + CO. The acetyl−vinoxy isomerization has been reported to have a high barrier of ~170 kJ/mol on the vinoxy side and ~200 kJ/mol on the acetyl side.[56,57] However, given that the average vibrational energy is only about 138 kJ/mol above the vinoxy zero-point level (see below), the vinoxy−acetyl isomerization is probably too slow to account for the rise of few tens of ps observed here.

**4.4. Competition between IVR and Dissociation: The Modified $S_1D$ Mechanism.** Having excluded the above seeming possibilities, we propose that the complex rising behavior of the methyl products is related to the scenario discussed in section 4.2, that is, IVR competes with the secondary dissociation in $CH_3CO(\tilde{X})$ and forbids the acetyl ground state from being ionized at the two-photon absorption level. According to the $S_1D$ mechanism, the vibrational energy deposited in $CH_3CO(\tilde{X})$ arises from the vibrational excitation in the primary dissociation and the electronic−vibrational energy conversion in the ultrafast $\tilde{A} \rightarrow \tilde{X}$ IC. The former can be estimated, on the average, to be ~68 kJ/mol based on the methyl product

**SCHEME 2: A Kinetic Representation of the Modified $S_1D$ Mechanism**

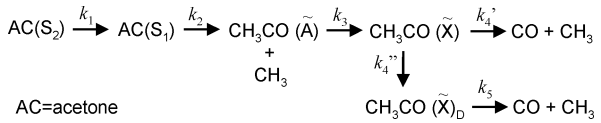


vibrational and kinetic energy distributions,[58] and the latter is simply the ~96 kJ/mol energy gap between the acetyl $\tilde{A}$ and $\tilde{X}$ states.[19] Thus, the total average vibrational energy available for the secondary dissociation in $CH_3CO(\tilde{X})$ amounts to ~164 kJ/mol, which is much higher than the C−C dissociation barrier of 71 ± 4 kJ/mol.[59] However, a great portion of the vibrational energy obtained via the $CH_3CO$ $\tilde{A} \rightarrow \tilde{X}$ IC is expected to be initially localized in the CCO bending mode because of the large structural change along this coordinate and the ultrafast nature (~100 fs) of the process. Thus, the redistribution of localized bending energy and the secondary dissociation may take place competitively, and both result in a reduction in the $CH_3CO^+$ signal (see section 4.2).

This complex dynamical process can be approximately represented by the kinetic model shown in Scheme 2, in which the hot $CH_3CO(\tilde{X})$ intermediate decays through two competing channels to produce the final products. The first one, $k_4'$, represents the dissociation originating from the phase space region directly connected to the dissociation channel, and the second one ($k_4''$) represents the CCO bending-energy relaxation followed by the subsequent secondary dissociation ($k_5$). The bend-relaxed intermediate, $CH_3CO(\tilde{X})_D$, is assumed to be "dark" to our probing scheme, and therefore, its decay does not appear in the observed acetyl transients. The observed $CH_3CO(\tilde{X})$ decay is thus governed by the combination of the two decay pathways (i.e., $k_4 = k_4' + k_4''$); whereas the rise of the secondary methyl fragment is composed of the two different temporal components arising from the two pathways. It should be emphasized here that the two-competing-steps description of the secondary dissociation is an oversimplified kinetic representation of the complex dynamics. It is proposed here only for the convenience of fitting the data.

The kinetics derived from this modified version of the $S_1D$ mechanism is the same as those obtained from the unmodified one for the initial state and intermediates, that is, all time constants obtained from fitting the parent and acetyl transients mentioned above are still valid. However, the decay of $CH_3CO(\tilde{X})$, which we have determined to be 6.2 ps, should be reinterpreted as the combination of the secondary dissociation and CCO bending relaxation (i.e., $k_4 = k_4' + k_4''$). Figure 10 shows the best fits of methyl transients to the modified $S_1D$ mechanism (Scheme 2). In these fits, we included one dissociative ionization, one primary methyl, and two secondary methyl components. All time constants ($\tau_1$, $\tau_2$, $\tau_3$, and $\tau_4 = 1/(k_4' + k_4'')$) obtained from fitting the parent and acetyl transients were fixed, while the rest of the parameters were varied during the fits. The time constant thus determined for the dark $CH_3CO(\tilde{X})_D$ dissociation ($\tau_5$) is ~25 ± 5 ps, which is much longer than the observed acetyl decay. It is apparent in Figure 10 that up to about 30 ps the methyl transient is well-described by the time constants derived from the parent and acetyl transients ($\tau_1$, $\tau_2$, $\tau_3$, and $\tau_4$), but an additional slower component is needed beyond 40 ps to describe the much slower rise. Thus, the observed temporal behaviors of all species involved in the reaction (i.e., the initial state, intermediates, and products) are all satisfactorily described by the same kinetic model using a single set of time constants. The amplitude ratio of the two secondary methyl components is about $A'/A'' = 3.1/1.0$, which

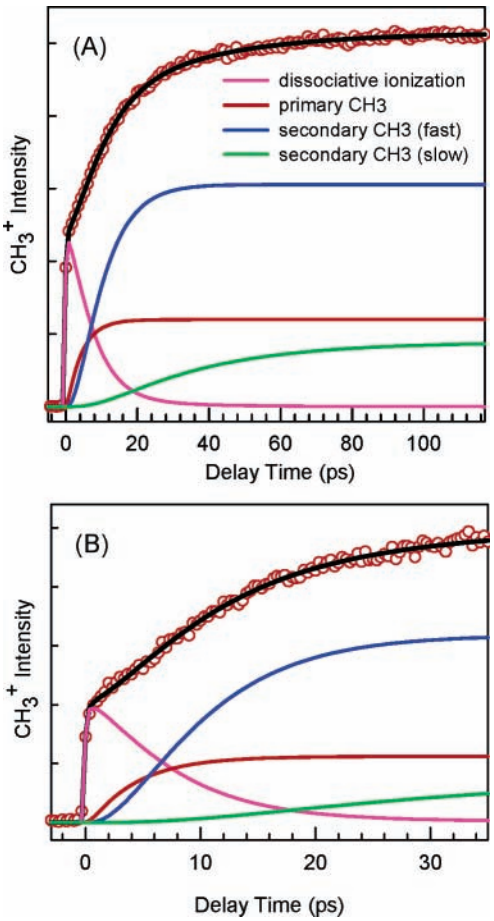


**Figure 10.** (A) Best fit of the 333.5-nm methyl transient to the modified $S_1D$ mechanism shown in Scheme 2. The black solid curve is the result of the fit, and the colored curves are the decomposed components. The time constant $\tau_5$ obtained from the fit was 25 ± 5 ps. All other time constants obtained from fitting the parent and acetyl transients were fixed during the fit. The traces of the decomposed components are color-coded as follows: dissociative ionization = pink; primary methyl = red; fast secondary methyl ($k_4'$) = blue; slow secondary methyl ($k_5$) = green. (B) Best fit to a short-time-scale methyl transient showing the quality of the fit in the early-time region. All time constants were fixed at the same values used in (A) during the fit.

translates to $\tau_4' = 8.2$ ps and $\tau_4'' = 25.5$ ps. The amplitude ratio of the primary to secondary methyl products is about 1:3 from the fit. Because photodissociation of acetone at 193 nm has been shown to produce $2CH_3 + CO$ with a quantum yield of nearly unity,[11,26] this ratio must be a consequence of REMPI probing via the $0_0^0$ transition and suggests that the secondary methyl is vibrationally much colder than the primary methyl.

A few points need to be mentioned here to clarify the model. First, the "dark" $CH_3CO(\tilde{X})_D$ in the kinetic model represents those acetyl radicals whose bending vibrational energy is drained out to below a certain threshold such that the vertical IP is too high for them to be ionized efficiently at the two-photon absorption level. While the energy localized in the bend is being dissipated into other modes, secondary dissociation also takes place. Those that dissociate prior to becoming dark are assigned to the $k_4'$ step in the model.

Second, the acetyl radicals are produced with a broad internal energy distribution, which should also result in a broad range of secondary dissociation rates. The much slower dissociation rate of the dark $CH_3CO(\tilde{X})_D$ is thus justified: because the acetyl radicals that dissociate in the first 6 ps ($1/(k_4' + k_4'')$) are those with higher internal energies, while those left behind (i.e., dark $CH_3CO(\tilde{X})_D$) contain less energy and thus dissociate much more

slowly. This evaporative cooling mechanism is further supported by the time-resolved kinetic energy distributions of the methyl products that will be presented in the following paper.[30] This effect and the very slow energy flow from the bending to other modes, which is comparable to the dissociation, justify the need to assign $CH_3CO(\tilde{X})_D$ as a kinetically distinct species, because once the bending relaxation completes, the acetyl ensemble contains a substantially lower average vibrational energy.

Finally, as stated above, the model implies that the bending vibration is not strongly coupled to other modes, such that the IVR is slower than or comparable to the dissociation. This is plausible, as the acetyl radical is a relatively small molecule with only six atoms. The vibrational level density is only about $(2 \times 10^3)/cm^{-1}$ even at the very high internal energy of ~164 kJ/mol. Because a large fraction of this level density arises from the low-frequency methyl torsion that is not expected to couple strongly with other modes of higher frequencies, the effective vibrational level density for IVR could be much lower. The relatively low-level density and possible weak couplings between modes could result in an IVR slower than the time scale of the reaction (~10 ps). This speculation is supported by the very large discrepancy between the observed and Rice−Ramsperger−Kassel−Marcus (RRKM) rates generally found in hot acetyl radical dissociation.[13,15,16,60] In the present case, simple RRKM calculations using the estimated vibrational energy in $CH_3CO(\tilde{X})$[58] and vibrational frequencies obtained by ab initio calculations[62] at the UB3LYP/6-311+G(d,p) level of theory gave a dissociation time constant as short as 70 fs, which deviates from the observed reaction times by at least 2 orders of magnitude!

**4.5. Vibrationally Excited Methyl Products.** The 333.5 nm probe laser detects the free methyl products through the $CH_3$ $3p\ ^2A_2'' \leftarrow 2p\ ^2A_2''\ 0_0^0$ transition. Owing to its intrinsic broad spectral width of ~2.5 nm, the 333.5 nm fs probe laser covers not only the entire rotational contour of the $0_0^0$ band but also the symmetric stretch $1_1^1$ hot band of the nascent methyl products.[10] However, Trentelman et al.[10] had shown that the $1_1$ level population is about 20 times smaller than the vibrational ground level, thus our 333.5 nm methyl transients mainly reflect the formation of vibrationless $CH_3$ products. On the other hand, the methyl transient probed at 329.5 nm via the $2_1^1$ transition represents the growth of the umbrella-mode excited methyl products. The 329.5 nm transient can be well-fitted using the same kinetic model (Scheme 2) discussed above with the same set of time constants, as shown in Figure 11. However, the relative amplitudes among components are different from those probed at 333.5 nm. Notably, the neutral methyl component is now comparable in size to the dissociative ionization component, indicating that umbrella-mode excited $CH_3$ is less populated than vibrationally cold products. Close inspections of the decomposed components from the fit revealed that the major reduction occurs in the secondary component, whereas the primary component does not decrease significantly. This suggests that the primary methyl is much more excited in the umbrella mode than the secondary methyl, qualitatively consistent with the ratio of the primary to the secondary components observed in the 333.5 nm transient.

Because the dissociative ionization component is nearly constant within the small spectral range (333.5−329.5 nm), the population ratio between the $CH_3$ $\nu = 0$ and $\nu_2 = 1$ levels can be estimated from the components resolved in the fits by using the dissociative ionization component as a reference and Franck−Condon factor corrections for the $0_0^0$ and $2_1^1$ transitions.[63] The analyses gave a population ratio of $CH_3$ ($\nu = 0$):

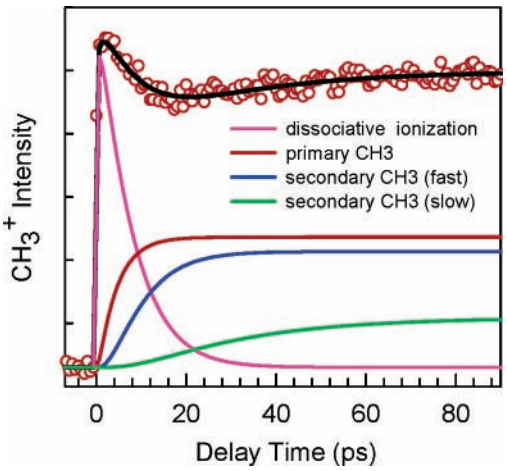


**Figure 11.** Best fit of the umbrella-mode excited methyl transient probed at 329.5 nm to the modified $S_1D$ mechanism shown in Scheme 2. The time constant $\tau_5$ obtained from the fit was within the uncertainty of that derived from the 333.5 nm transient shown in Figure 10. All other time constants obtained from fitting the parent and acetyl transients were fixed during the fit.

$CH_3$ ($\nu_2 = 1$) = 1:0.47 for all methyl products. This ratio is consistent with the ratio of 1:0.41 reported by Trentelman et al. using nanosecond (ns) laser REMPI detection.[10] Population analyses of methyl radicals using ns laser REMPI are known to be complicated by the predissociative nature of the intermediate (stepping) states. However, this should not be problematic in the present fs laser REMPI detection, provided that the probe-laser pulse width (~100 fs) is much shorter than the stepping-state lifetimes. This suggests that the population ratios reported by Trentelman et al.[10] were not severely influenced by predissociation. In fact, these authors have provided convincing arguments inferring that the predissociation rates of the stepping states they reached are very similar.[10]

It is also possible to estimate the population ratios for the primary and secondary methyl fragments from the decomposed components: $CH_3$ ($\nu = 0$):$CH_3$ ($\nu_2 = 1$) = 1:0.84 for the primary methyl, and $CH_3$ ($\nu = 0$):$CH_3$ ($\nu_2 = 1$) = 1:0.36 for the secondary methyl. Note that the primary methyl only contributes about 25% in the total $CH_3$ ($\nu = 0$) signal, and therefore, the average ratio (1:0.47) is overwhelmed by the secondary methyl which constitutes 75% of the $CH_3$ ($\nu = 0$) signal. Assuming that a Boltzmann distribution exists in the methyl fragments, these ratios translate to $T_{\nu_2} = 4000$ K and $\langle E_v \rangle(\nu_2) = 29.5$ kJ/mol for the primary methyl and $T_{\nu_2} = 870$ K and $\langle E_v \rangle(\nu_2) = 4.1$ kJ/mol for the secondary methyl. Because nonstatistical state distributions are expected for fragments produced in ultrafast dissociation, these temperatures and energies should be used with caution. Nevertheless, these results clearly show that the umbrella mode is highly excited in the primary methyl, whereas it is only moderately excited in the secondary methyl. It is likely that, during the rapid primary dissociation of ~0.6 ps, a major fraction of the available energy is deposited in the umbrella mode because of a large structural change in the $CH_3$ moiety along that coordinate. On the other hand, the secondary dissociation takes a much longer time, which allows the energy to be randomized among all modes when crossing the transition-state region. Moreover, ab initio calculations have shown that the transition state for $CH_3CO$ C−C dissociation has similar local structures and frequencies in the $CH_3$ moiety to those in the final product.[56] These factors make the secondary methyl much colder than the primary one, at least in the umbrella mode. Because vibrational excitation in

other modes may be very different, we cannot say anything about the total vibrational energy in both fragments.

The internal energy deposition in the methyl products upon photodissociation of acetone at 193 nm has been measured by several groups;[8,10,64] however, the results are controversial. Trentelman et al.[10] measured REMPI spectra of nascent $CH_3$ products and concluded that $\langle E_{vib}\rangle = 5$ kJ/mol and $\langle E_{rot}\rangle = 6$ kJ/mol. In view of the present results, it is likely that Trentelman et al. underestimated the vibrational energy in methyl fragments, because the two components were not resolved in their experiments, and therefore, the REMPI spectra were dominated by the much colder secondary methyl for low vibrational levels. Hall et al.[64] employed diode laser transient absorption spectroscopy to study the photodissociation of acetone-$d_6$ and found that only 6% of the $CD_3$ fragments are in the vibrational ground state, indicating an extremely hot methyl radical production. However, the much lower frequencies in $CD_3$ would probably dramatically affect the vibrational excitation upon dissociation, and therefore, a direct comparison with the acetone-$h_6$ results is not justified. Donaldson and Leone[8] measured the time-resolved IR emission spectra of methyl products and concluded that $\langle E_{vib}\rangle(\nu_3) = 16$ kJ/mol and $\langle E_{rot}\rangle = 19$ kJ/mol in at least one methyl. This result indicated a moderate excitation in the doubly degenerate $\nu_3$ mode in at least one $CH_3$, presumably the primary one, and is probably more consistent with present results.

**4.6. Primary and Secondary Dissociation Dynamics.** The present results and analyses have revealed a detailed photodissociation dynamics of acetone excited at 195 nm. Upon photoexcitation to its $S_2$ state, acetone first undergoes a relatively slow IC (~4 ps) to the lower $S_1$ state. With 250 kJ/mol vibrational energy, the hot acetone $S_1$ state rapidly undergoes an adiabatic dissociation along the α-CC coordinate to produce a methyl radical and an electronically excited acetyl radical, $CH_3CO(\tilde{A})$. Our results indicated that this process takes about $0.6 \pm 0.2$ ps, which is rather rapid for adiabatic dissociation on a bound surface. This could be due to the very high vibrational energy deposited via $S_2 \rightarrow S_1$ IC and the relatively low barrier to α-CC dissociation of about 77 kJ/mol on the $S_1$ surface.[17,20] Simple RRKM calculations using this barrier height and the frequencies for the minimum and transition state of the $T_1$ surface obtained by ab initio calculations[62] at the UB3LYP/6-311G(d) level of theory gave a dissociation time constant of 0.95 ps, roughly consistent with the experimental value. Although nonstatistical behavior is expected owing to the ultrafast time scale involved, the simple RRKM rate calculations suggested that our assignment of <1 ps adiabatic dissociation rate on the $S_1$ surface is reasonable.

The very rapid adiabatic dissociation on the $S_1$ surface is the key step causing the reaction to follow the $S_1D$ pathway instead of the $T_1D$ mechanism, as it is probably much faster than the $S_1 \rightarrow T_1$ ISC. Because acetone $S_1$ ISC rates at high energies have not been well determined, it is necessary to comment on its significance here. Fluorescence lifetimes ($\tau_f$) of jet-cooled acetone have been measured for the $S_1$ low-energy region.[24,65] At the $S_0-S_1$ band origin (328.6 nm), $\tau_f$ was observed to be ~1 μs and was attributed to $S_1 \rightarrow S_0$ IC.[65] The fluorescence lifetime increases slowly with the excitation energy up to about 2300 $cm^{-1}$ above the origin (~305 nm), where $\tau_f$ suddenly decreases to <10 ns within an energy range of ~100 $cm^{-1}$.[23,24] This observation has been ascribed to the dissociation threshold on the $T_1$ surface.[23,24] A recent fs pump−probe MPI experiment using 307 nm excitation has confirmed the ns time scale for the $S_1$ lifetime in this energy region.[17] Reliable measurements at higher energies are scarce. Early fluorescence measurements[66] in bulk acetone vapor (20 Torr) gave $\tau_f < 1.6$ ns for excitation at 260 nm. A more recent measurement[67] using a 30 ps 266 nm laser for excitation and a streak camera for detection yielded $\tau_f = 1.05$ ns and $\tau_f = 0.75$ ns for acetone vapors (~15 Torr) at 323 and 723 K, respectively. In the latter case, the average excitation energy is equivalent to excitation at 240 nm from the vibrational ground state. In contrast to these fluorescence data, two groups have reported an ultrafast (<200 fs) $S_1$ lifetime at 260 nm using fs pump−probe mass-selected MPI.[14−16] It has been argued that the ~1 ns fluorescence lifetime measured in bulk vapors may not be collision-free.[16] However, the mean collision times in these bulk vapor measurements are about an order of magnitude greater than the observed fluorescence lifetimes. Even if collisions took place in these measurements, the initially excited $S_1$ levels still have to live long enough to be perturbed by collisions, which occur with an average interval of ~10 ns! If the lifetimes were shorter than 200 fs, the initially excited $S_1$ levels at 260 nm would not have any chance to collide with other molecules, and no fluorescence can be observed in the aforementioned bulk vapor experiments.[66,67] Shibata and Suzuki[68] studied the acetone $S_1$ photodissociation at 253 nm using fs photofragment ion imaging and concluded that the acetone $S_1$ state excited at this wavelength is much longer than 15 ps.[69] Beyond this energy region, there exists no experimental data about the $S_1$ lifetime. However, judging from the above data, it is unlikely that ISC can become competitive to the observed $S_1$ primary dissociation of 0.6 ps at the present excitation energy (195 nm).

Following the primary dissociation, the resultant $CH_3CO(\tilde{A})$ then quickly converts to the acetyl ground state, $CH_3CO(\tilde{X})$, possibly via the CCO bending motion. Our analyses indicated that this process takes about 100 fs. This time scale is consistent with the near-degeneracy of the acetyl $\tilde{A}$ and $\tilde{X}$ states at the linear configuration (see Figures 1 and 8),[19] which makes the IC between the two states facile. Houston's group has carried out extensive spectroscopic studies on the analogous system of HCO.[70] The observed linewiths of the diffuse HCO $\tilde{X} \rightarrow \tilde{A}$ vibronic transitions were interpreted as radiationless transition rates and yield upper HCO $\tilde{A}$-state lifetimes ranging from 70 to 700 fs,[70] consistent with the time scale determined here for the $CH_3CO$ $\tilde{A}$-state decay. The $CH_3CO$ $\tilde{A} \rightarrow \tilde{X}$ IC step transforms 96 kJ/mol of electronic energy into vibrational energy and ensures all $CH_3CO(\tilde{X})$ thus produced possess internal energy higher than the C−C dissociation barrier (~71 kJ/mol),[59] which is consistent with the near-unity three-body dissociation yield.

Following the ultrafast IC, the hot $CH_3CO(\tilde{X})$ contains totally ~164 kJ/mol of vibrational energy,[58] as discussed in section 4.4, and subsequently undergoes a secondary dissociation to produce CO and secondary $CH_3$ via a low barrier. The dissociation of hot acetyl radicals has been a subject of interest for many years.[13−16,56,59,60,71,72] The barrier to C−C dissociation has been experimentally determined to be $71 \pm 4$ kJ/mol,[59] and the exit barrier (i.e., the barrier to recombination) has been estimated to be 38 kJ/mol based on the forward barrier and thermochemical data.[56] Several groups have reported observations of nonstatistical behaviors in hot acetyl radical dissociation.[13,16,60] In the present case, although the acetyl transients suggested that hot $CH_3CO(\tilde{X})$ decays exponentially in 6.2 ps, the analyses of the methyl transients have revealed that the secondary dissociation follows a very complex dynamics, and an additional rise of about 25 ps was identified. These time scales (6.2 and 25 ps) are ~2−3 orders of magnitude longer than that predicted by simple RRKM calculations described in

the previous section, indicating that a slow IVR dominates the reaction. Because a major fraction of the ~164 kJ/mol vibrational energy[58] is expected to be initially trapped in the CCO bending mode, we speculate that the main reason for this large discrepancy is a very weak coupling between the CCO bend and the other modes including the dissociation coordinate.[13] This may explain the non-RRKM behavior generally observed in the acetyl dissociation, regardless of the method of preparation.[13,16,60]

Ito et al.[73] have studied the dissociation dynamics of the acetyl radical with the classical trajectory method using the electronic model Hamiltonian based on ab initio calculations. They reported that "the energy of the CCO bending excitation does not efficiently transfer into the dissociation coordinate (C−C) over the time period of 30 ps".[73] Peña-Gallego et al.[74] have carried out the classical trajectory and statistical variational efficient microcanonical sampling transition state theory calculations (EMS-TST) to investigate the unimolecular dissociation of the acetyl radical. At an internal energy (~160 kJ/mol) close to the present case, the two approaches predicted a dissociation time constant of about 1.6 ps.[74] More importantly, they have shown that the reaction exhibits an intrinsic non-RRKM behavior at high energies (>170 kJ/mol) where the trajectory decay curves are found to be nonexponential. However, it is also important to note that in the latter study[74] the CCO bending mode was found to enhance the dissociation. Our observed rate is lower than the value predicted by Peña-Gallego et al.,[74] probably because in the present case the acetyl radicals are produced with a very broad internal energy distribution, and the initial vibrational-state distribution is not uniform. These theoretical results indicate that the dissociation of acetyl radicals is nonstatistical and are consistent with the nonexponential rise observed for the secondary methyl.

The very high internal energy, low dissociation barrier, nonuniform initial vibrational-state distribution, and slow IVR that all coexist in the hot acetyl radical thus produce a very complex secondary dissociation dynamics. There are two types of initial vibrational-state distributions in the hot acetyl radical: One is more or less randomly distributed among all modes and arises mostly from the vibrational excitation during the primary dissociation; the other is very much localized in the CCO bend and is mostly the result of the $\tilde{A} \rightarrow \tilde{X}$ IC. While the energy localized in the bending mode slowly flows into other modes via IVR, dissociation also occurs simultaneously. Because the bending mode is not strongly coupled to the dissociation coordinate, the energy available for dissociation in all other modes is much lower, resulting in a much lower rate than that predicted by simple RRKM calculations. Because IVR and dissociation occurs competitively, the surviving acetyl radicals contain considerably less energy in the bending mode at the later stage (>6 ps) of the reaction, which prevent them from being detected by the probe laser. The above description of the dynamics has to be convoluted with the broad internal energy distribution of the acetyl intermediates. Thus, those that dissociate in the early stage (<6 ps) of the reaction are those containing higher internal energy; whereas those left behind (i.e., the "dark" acetyl radicals) contain not only less bending energy but also less total internal energy due to the evaporative cooling effect and therefore dissociate much more slowly with a time constant of ~25 ps.

## 5. Conclusions

In this work, we have provided experimental evidence to support the validity of the $S_1$D mechanism by using femtosecond time-resolved mass-selected mulitiphoton ionization spectroscopy. The mass-selected transients of the initial state (parent), intermediate (acetyl), and products (methyl) can all be well-fitted to the modified $S_1$D mechanism (Scheme 2) using a single set of time constants. On the other hand, the old $T_1$D mechanism produced unsatisfactory fits, especially for the acetyl intermediate. The analyses have revealed the following dynamics: Upon photoexcitation of acetone at 195 nm, the initially excited $S_2$ state first undergoes a relatively slow IC (~4 ps) to the highly vibrationally excited region of the $S_1$ state. With 250 kJ/mol vibrational energy, the $S_1$ state rapidly undergoes an adiabatic dissociation along the α-CC coordinate in about 0.6 ps to produce a methyl radical and an electronically excited acetyl radical, $CH_3CO(\tilde{A})$. The latter rapidly undergoes an internal conversion to its ground state, $CH_3CO(\tilde{X})$, in about 100 fs. The resultant hot acetyl ground state then undergoes a secondary dissociation to produce another methyl radical and a carbon monoxide via a complex dynamics. The hot acetyl radical decays in ~6.2 ps within our detection window, but the formation of the secondary methyl can be approximately characterized by the combination of a 6.2 ps rise and an additional slower rise of 25 ps. The complex behavior of the secondary dissociation is the manifestation of competition between dissociation and slow IVR. Analyses of the methyl transients probed via $CH_3$ $0_0^0$ and $2_1^1$ transitions suggested that the primary methyl is vibrationally hotter than the secondary methyl. The umbrella mode was found to be highly excited in the primary methyl, whereas it is only moderately excited in the secondary methyl.

Although the results and analyses presented here suggested that the $T_1$D mechanism is not adequate in describing the photodissociation of acetone at 195 nm, it should be noted that the two mechanisms are simply competing pathways branching at the $S_1$ state. For excitation into the low-energy region below the $S_1$ adiabatic dissociation threshold (~270 nm), the $S_1 \rightarrow T_1$ ISC dominates, and the reaction follows the conventional route to dissociate on the $T_1$ surface. For excitation above the $S_1$ dissociation threshold, the adiabatic dissociation rate increases with the excitation energy, and the two pathways compete.[20] When the excitation is much higher than the dissociation threshold, as in the present case, the $S_1$ adiabatic dissociation is much faster than the $S_1 \rightarrow T_1$ ISC, and the reaction is dominated by the $S_1$D mechanism. It is interesting to note that the photodissociation dynamics of $S_2$ acetone is governed by the very large energy gap between the $S_2$ and $S_1$ states. This large energy gap results in a relatively slow $S_2 \rightarrow S_1$ IC and a very rapid adiabatic dissociation on the $S_1$ surface, which surpasses the $S_1$ ISC and guides the system to follow the $S_1$D mechanism.

It is also important to note here that the differentiation between the $T_1$D and $S_1$D mechanisms described in this work was based on simple kinetic modeling under the assumption that the internally converted hot $S_1$ state was not detected. Although this assumption is supported by experimental evidence as well as common theoretical considerations, doubts might still exist. In the following paper, we will present results obtained by femtosecond time-resolved photofragment translational spectroscopy, which provides nearly independent evidence to further support the dominance of the $S_1$D mechanism and aid in elucidating the detailed dynamics.

**Acknowledgment.** This work was supported by the MOE Program for Promoting Academic Excellence of Universities (89-FA04-AA) and by the National Science Council of Taiwan, R. O. C. (NSC 92-2113-M-007-052).

## References and Notes


(1) Lee, E. K. C.; Lewis, R. S. *Adv. Photochem.* **1980**, *12*, 1; and references therein.

(2) Reinsch, M.; Klessinger, M. *J. Phys. Org. Chem.* **1990**, *3*, 81.

(3) Haas, Y. *Photochem. Photobiol. Sci.* **2004**, *3*, 6; and references therein.

(4) Arnold, F.; Burger, V.; Droste-Fanke, B.; Grimm, F.; Krieger, A.; Schneider, J.; Stilp, T. *Geophys. Res. Lett.* **1997**, *24*, 3017.

(5) Arnold, S. R.; Chipperfield, M. P.; Blitz, M. A.; Heard, D. E.; Pilling, M. J. *Geophys. Res. Lett.* **2003**, *31*, L07110.

(6) Baba, M.; Shinohara, N.; Nishi, N.; Hirota, N. *Chem. Phys.* **1984**, *83*, 221.

(7) Woodbridge, E. L.; Fletcher, T. R.; Leone, S. R. *J. Phys. Chem.* **1988**, *92*, 5387.

(8) Donaldson, D. J.; Leone, S. R. *J. Chem. Phys.* **1986**, *85*, 817.

(9) Gaines, G. A.; Donaldson, D. J.; Strickler, S. J.; Vaida, V. *J. Phys. Chem.* **1988**, *92*, 2762.

(10) Trentelman, K. A.; Kable, S. H.; Moss, D. B.; Houston, P. L. *J. Chem. Phys.* **1989**, *91*, 7498.

(11) Waits, L. D.; Horwitz, R. J.; Guest, J. A. *Chem. Phys.* **1991**, *155*, 149.

(12) North, S. W.; Blank, D. A.; Gezelter, J. D.; Longfellow, C. A.; Lee, Y. T. *J. Chem. Phys.* **1995**, *102*, 4447.

(13) Kim, S. K.; Pedersen, S.; Zewail, A. H. *J. Chem. Phys.* **1995**, *103*, 477.

(14) Zhong, Q.; Poth, L.; Castleman, A. W., Jr. *J. Chem. Phys.* **1999**, *110*, 192.

(15) Owrutsky, J. C.; Baronavski, A. P. *J. Chem. Phys.* **1998**, *108*, 6652.

(16) Owrutsky, J. C.; Baronavski, A. P. *J. Chem. Phys.* **1999**, *110*, 11206.

(17) Diau, E. W. G.; Kötting, C.; Zewail, A. H. *ChemPhysChem* **2001**, *2*, 273.

(18) Diau, E. W. G.; Kötting, C.; Zewail, A. H. *ChemPhysChem* **2001**, *2*, 294.

(19) Diau, E. W. G.; Kötting, C.; Sølling, T. I.; Zewail, A. H. *ChemPhysChem* **2002**, *3*, 57.

(20) Sølling, T. I.; Diau, E. W. G.; Kötting, C.; De Feyter, S.; Zewail, A. H. *ChemPhysChem* **2002**, *3*, 79.

(21) Hansen, D. A.; Lee, E. K. C. *J. Chem. Phys.* **1975**, *62*, 183.

(22) Baba, M.; Hanazaki, I.; Nagashima, U. *J. Chem. Phys.* **1985**, *82*, 3938.

(23) Zuckermann, H.; Schmitz, B.; Yaas, Y. *J. Phys. Chem.* **1988**, *92*, 4835.

(24) Zuckermann, H.; Schmitz, B.; Yaas, Y. *J. Phys. Chem.* **1989**, *93*, 4083.

(25) Robin, M. B.; Kuebler, N. A. *J. Mol. Spectrosc.* **1970**, *33*, 274.

(26) Lightfoot, P. D.; Kirwan, S. P.; Pilling, M. J. *J. Phys. Chem.* **1988**, *92*, 4938.

(27) Takahashi, K.; Nakayama, T.; Matsumi, Y.; Osamura, Y. *J. Phys. Chem. A* **2004**, *108*, 8002.

(28) Chen, W. K.; Ho, J. W.; Cheng, P. Y. *Chem. Phys. Lett.* **2003**, *380*, 411.

(29) Hudgens, J. W.; DiGiuseppe, T. G.; Lin, M. C. *J. Chem. Phys.* **1983**, *79*, 571.

(30) Chen, W. K.; Cheng, P. Y. *J. Phys. Chem. A* **2005**, *109*, 6818.

(31) Brint, P.; O'Toole, L.; Couris, S.; Jardine, D. *J. Chem. Soc., Faraday Trans.* **1991**, *87*, 2891.

(32) McDiarmid, R. *J. Chem. Phys.* **1991**, *95*, 1530.

(33) Cheng, P. Y.; Zhong, D.; Zewail, A. H. *J. Phys. Chem.* **1995**, *99*, 15733.

(34) Cheng, P. Y.; Zhong, D.; Zewail, A. H. *Chem. Phys. Lett.* **1995**, *242*, 369.

(35) Bixon, M.; Jortner, J. *J. Chem. Phys.* **1968**, *48*, 715.

(36) The $S_1$ component may be similar to the $S_2$ component only if the $S_1$ state decays in a time scale much faster than our pulse width, e.g., due to dissociation in the $S_1$ state. However, RRKM calculations and the rise of the methyl products observed in the methyl transients and in the time-resolved kinetic-energy distributions described in the following paper indicate that the dissociation in the $S_1$ state is at least three times slower than our time resolution (~200 fs) and should be resolvable.

(37) Stolow, A.; Bragg, A. E.; Neumark, D. M. *Chem. Rev.* **2004**, *104*, 1719; and references therein.

(38) Hayden, C. C.; Chandler, D. W. *J. Phys. Chem.* **1995**, *99*, 7897.

(39) Cyr, D. R.; Hayden, C. C. *J. Chem. Phys.* **1996**, *104*, 771.

(40) Stert, V.; Farmanara, P.; Radloff, W. *J. Chem. Phys.* **2000**, *112*, 4460.

(41) Radloff, W.; Stert, V.; Freudenberg, T.; Hertel, I. V.; Jouvet, C.; Dedonder-Lardeux, C.; Solgadi, D. *Chem. Phys. Lett.* **1997**, *281*, 20.

(42) Radloff, W.; Freudenberg, T.; Ritze, H. H.; Stert, V.; Noack, F.; Hertel, I. V. *Chem. Phys. Lett.* **1996**, *261*, 301.

(43) Farmanara, P.; Stert, V.; Radloff, W.; Hertel, I. V. *J. Phys. Chem. A* **2001**, *105*, 5613.

(44) Schultz, T.; Quenneville, J.; Levine, B.; Toniolo, A.; Martinez, T. J.; Lochbrunner, S.; Schmitt, M.; Shaffer, J. P.; Zgierski, M. Z.; Stolow, A. *J. Am. Chem. Soc.* **2003**, *125*, 8089.

(45) Schultz, T.; Fischer, I. *J. Chem. Phys.* **1997**, *107*, 8197.

(46) Schultz, T.; Fischer, I. *J. Chem. Phys.* **1998**, *109*, 5812.

(47) Diau, E. W. G.; De Feyter, S.; Zewail, A. H. *J. Chem. Phys.* **1999**, *110*, 9785.

(48) Matsumoto, Y.; Kim, S. K.; Suzuki, T. *J. Chem. Phys.* **2003**, *119*, 300.

(49) Kang, H.; Jung, B.; Kim, S. K. *J. Chem. Phys.* **2003**, *118*, 6717.

(50) Clara, M.; Hellerer, T.; Neusser, H. *J. Appl. Phys. B* **2000**, *71*, 431.

(51) Pedersen, S.; Bañares, L.; Zewail, A. H. *J. Chem. Phys.* **1992**, *97*, 8801.

(52) Fuss, W.; Schikarski, T.; Schmid, W. E.; Trushin, S. A.; Hering, P.; Kompa, K. L. *J. Chem. Phys.* **1997**, *106*, 2205.

(53) Loettgers, A.; Untch, A.; Keller, H.; Schinke, R.; Werner, H.; Bauer, C.; Rosmus, P. *J. Chem. Phys.* **1997**, *106*, 3186.

(54) Lias, S. G.; Bartmess, J. E.; Liebman, J. F.; Holmes, J. L.; Levin, R. D.; Mallard, W. G. *J. Phys. Chem. Ref. Data* **1988**, *17*, 1.

(55) Chen, W. K.; Ho, J. W.; Cheng, P. Y. To be published.

(56) Mordaunt, D. H.; Osborn, D. L.; Neumark, D. M. *J. Chem. Phys.* **1998**, *108*, 2448.

(57) Miller, J. L.; McCunn, L. R.; Krisch, M. J.; Butler, L. J.; Shu, J. *J. Chem. Phys*. **2004**, *121*, 1830.

(58) At 195 nm excitation, the available energy for primary dissociation on the $S_1$ surface is about 168 kJ/mol. A very simple statistical model can be used to estimate average vibrational energy deposited in the fragments by assuming that the available energy is equally partitioned into all modes during the reaction, which yields 84 kJ/mol for the average vibrational energy in acetyl radical. One can improve the accuracy of this simple approach by leaving out the degrees of freedom in which the partitioned energies have been determined or estimated well. In our case, the rotational energies of primary methyl and acetyl radicals have been estimated to be 6 kJ/mol.[10] The total kinetic energy release of the primary dissociation has been determined to be 31 kJ/mol, as will be described in the following paper.[30] There are 24 vibrational modes in acetone; 6 of them transform into product translation and rotation upon dissociation, leaving 18 modes in the 2 counter fragments. Because the umbrella-mode vibrational energy in the primary methyl product has also been estimated to be about 29.5 kJ/mol (see section 4.5), it can also be left out. Thus, there is only 95.5 kJ/mol of energy left to be equally distributed among the rest of 17 vibrational modes in 2 fragments, and the simple statistical model predicts that ~68 kJ/mol of vibrational energy resides in the acetyl radical.

(59) North, S.; Blank, D. A.; Lee, Y. T. *Chem. Phys. Lett*. **1994**, *224*, 38.

(60) Shibata, T.; Li, H.; Katayanagi, H.; Suzuki, T. *J. Phys. Chem. A* **1998**, *102*, 3643.

(61) Kim, S. K.; Guo, J.; Baskin, J. S.; Zewail, A. H. *J. Phys. Chem.* **1996**, *100*, 9202.

(62) All ab initio calculations described in this work were carried out with the *Gaussian 98* program suite: Frisch, M. J.; Trucks, G. W.; Schlegel, H. B.; Scuseria, G. E.; Robb, M. A.; Cheeseman, J. R.; Zakrzewski, V. G.; Montgomery, J. A., Jr.; Stratmann, R. E.; Burant, J. C.; Dapprich, S.; Millam, J. M.; Daniels, A. D.; Kudin, K. N.; Strain, M. C.; Farkas, O.; Tomasi, J.; Barone, V.; Cossi, M.; Cammi, R.; Mennucci, B.; Pomelli, C.; Adamo, C.; Clifford, S.; Ochterski, J.; Petersson, G. A.; Ayala, P. Y.; Cui, Q.; Morokuma, K.; Malick, D. K.; Rabuck, A. D.; Raghavachari, K.; Foresman, J. B.; Cioslowski, J.; Ortiz, J. V.; Stefanov, B. B.; Liu, G.; Liashenko, A.; Piskorz, P.; Komaromi, I.; Gomperts, R.; Martin, R. L.; Fox, D. J.; Keith, T.; Al-Laham, M. A.; Peng, C. Y.; Nanayakkara, A.; Gonzalez, C.; Challacombe, M.; Gill, P. M. W.; Johnson, B. G.; Chen, W.; Wong, M. W.; Andres, J. L.; Head-Gordon, M.; Replogle, E. S.; Pople, J. A. *Gaussian 98*, revision A.9; Gaussian, Inc.: Pittsburgh, PA, 1998.

(63) Ogoralek, R.; Haerri, H. P.; Hall, G. E.; Houston, P. L. *J. Chem. Phys.* **1989**, *90*, 4222.

(64) Hall, G. E.; Vanden Bout, D.; Sears, T. J. *J. Chem. Phys.* **1991**, *94*, 4182.

(65) Anner, O.; Zuckermann, H.; Haas, Y. *J. Phys. Chem.* **1985**, *89*, 1336.

(66) Breuer, G. M.; Lee, E. K. C. *J. Phys. Chem*. **1971**, *75*, 989.

(67) Ossler, F.; Alden, M. *Appl. Phys. B* **1997**, *64*, 493.

(68) Shibata, T.; Suzuki, T. *Chem. Phys. Lett.* **1996**, *262*, 115.

(69) The transient reported in ref 50 was "flat" up to 15 ps; hence, the lifetime should be at least 10 times longer.

(70) Loison, J.; Kable, S. H.; Houston, P. L.; Burak, I. *J. Chem. Phys.* **1991**, *94*, 1796.

(71) Deshmukh, S.; Myers, J. D.; Xantheas, S. S.; Hess, W. P. *J. Phys. Chem.* **1994**, *98*, 12535.

(72) Kroger, P. M.; Riley, S. J. *J. Chem. Phys.* **1977**, *67*, 4483.

(73) Ito, M.; Nanbu, S.; Aoyagi, M. *Inst. Mol. Sci. Annu. Rev.* **1998**, *VIII-A-3*, 176.

(74) Peña-Gallego, A.; Martínez-Núñez, E.; Vázquez, S. A. *J. Chem. Phys.* **1999**, *110*, 11323.